Eletrônica de Potência
Open Journal of Power Electronics

Received July 29, 2024; accepted November 20, 2024; Date of publication December 03, 2024.
The review of this paper was arranged by Associate Editor Margarita Norambuena and Editor-in-Chief Heverton A. Pereira.

Digital Object Identifier http://doi.org/10.18618/REP.e202452

Sensorless MPPT Algorithms for PV Systems in Partially Shaded Scenarios

Guilherme M. S. Martines[1], Moacyr A. G. de Brito[1], Edson A. Batista[1], Ruben B. Godoy[1], Tiago H. A. Mateus[1]

[1] Federal University of Mato Grosso do Sul - UFMS, Electrical Engineering Department, Faculty of Engineering, Architecture and Urbanism and Geography – FAENG, Campo Grande – MS, Brazil.

e-mail: guilherme.martines@ufms.br; moacyr.brito@ufms.br; edson.batista@ufms.br; ruben.godoy@ufms.br; tiago.mateus@ufms.br

ABSTRACT This manuscript presents current sensorless algorithms for maximum power point tracking (MPPT) in partially shaded photovoltaic (PV) systems. The necessity of a current sensor is eliminated with the use of mathematical modeling of the power electronics converter. This approach significantly reduces the implementation cost and the inherent disadvantages in the current sensor circuitry. MPPT techniques based on soft computing are employed, in addition to Perturb and Observe (P&O), due to their ability to explore a larger search space. This feature is advantageous because it minimizes convergence risk to a local maximum, a limitation of traditional techniques. Simulation and experimental results are presented and each algorithm is evaluated through different metrics, such as search time for the global maximum power point (GMPP) and efficiency. The tests consider dynamic irradiance profiles, producing a tracking factor (TF) above 99% and a remarkable fast convergence time.

KEYWORDS MPPT, sensorless, metaheuristic, reduced cost, partial shading conditions, photovoltaic arrays.

I. INTRODUCTION

Environmental conditions, such as irradiance (W/m^2) and temperature (°C), directly impact the nonlinear Power-Voltage (P-V) and Current-Voltage (I-V) curves of photovoltaic systems [1]. Under uniform irradiance conditions, these curves exhibit a single point of maximum power (MPP), as illustrated in Figure 1(a). To ensure optimal energy utilization, it is essential to maintain the photovoltaic system at the optimum operating point. To achieve this, a maximum power point tracking algorithm (MPPT) is employed. This algorithm controls a power electronics converter by adjusting the impedance observed by the photovoltaic module through voltage or current variations and, finally, the duty cycle of the converter.

The literature presents a wide range of MPPT algorithms, which can be categorized into traditional methods, artificial intelligence (AI) methods, metaheuristic methods, and hybrid methods. Traditional methods, such as Perturb and Observe (P&O), Incremental Conductance (IC), and Hill Climb (HC), perform well exclusively under uniform conditions [2, 3, 4]. However, they are not efficient in tracking under partial shading conditions, where the P-V and I-V characteristic curves exhibit multiple local maxima (LMPPs) and only one global maximum power point (GMPP), as depicted in Figure 1(b) [5, 6]. AI methods [7,8] perform better in tracking MPP under shading, but require greater computational burden and extensive training. Metaheuristic techniques can handle nonlinear optimization problems with computational simplicity, enabling a broad search for the MPP across the characteristic curves, and reducing the probability of converging to a local maximum. Hybrid methods are combinations of intelligent and conventional methods. In [9], a new algorithm is proposed that combines the fast response time of a conventional algorithm with the broad search space of a metaheuristic technique, thereby enhancing efficiency under partial shading conditions.

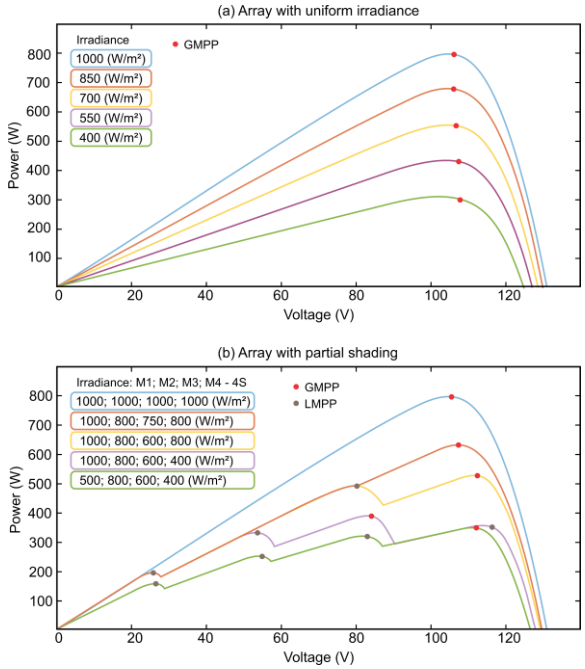

FIGURE 1. PxV curves. (a) with uniform irradiance, (b) with partial shading.

Many MPPT techniques commonly rely on current and voltage sensors. Removing the current sensor can offer several benefits, including reduced costs, lower computational data storage requirements, and improved system reliability [10]. Additionally, it helps avoid issues associated with Hall effect sensors, such as magnetic interference and measurement accuracy problems. Incorporating additional sensors into the prototype requires

not only the sensors themselves but also the conditioning circuitry and a controller with an additional analog-to-digital converter (ADC). A high sampling rate ADC is commonly necessary. Furthermore, current sensor circuitry is susceptible to switching noise, which can degrade controller performance.

In this manuscript, global and hybrid algorithms with only one voltage sensor at the input are proposed. The need for a current sensor is eliminated as the MPPT algorithms incorporate mathematical formulations that enable the estimation of current measurements, and a controller is integrated into the algorithms to increase energy conversion effectiveness. The idea was first presented at the Brazilian Power Electronics Conference – COBEP 2023 [11] in an initial stage with simulation results. In this version, not only simulations but also experimental evaluations are performed with deeper discussions of flowcharts and coefficients tuning, and the results demonstrate that the proposed algorithms can track efficiently in the face of shading and maintain the same performance and dynamic response comparable to techniques that use both voltage and current sensors.

II. PROPOSED METHODS

Figure 2 illustrates the main concept of the proposed algorithms. At its core, it employs a global MPPT approach. Additionally, hybrid algorithms are derived to further enhance performance. The input is the measured PV voltage and the output is the PV reference voltage, which is tracked by the power electronics converter with the use of a PI controller. The PI controller generates the duty cycle of the converter, which is used as feedback to estimate the PV current. Hence, observing the complete algorithm, the input is only the PV voltage (V_{PV}) and the output is the duty cycle (D).

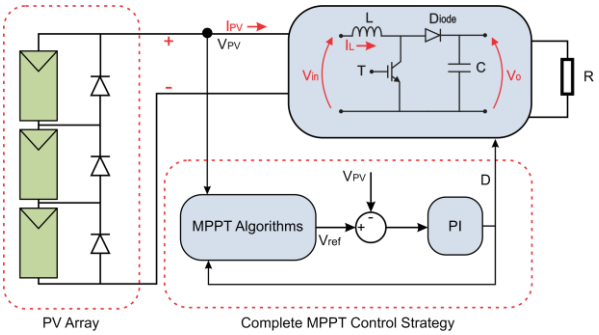

FIGURE 2. Simplified model of the MPPT Algorithms.

The implemented global algorithms are inspired by natural phenomena: they mimic natural processes to provide optimal solutions to global optimization problems. In this work, three distinct bioinspired techniques were employed. The first is the particle swarm optimization (PSO) algorithm, which draws inspiration from the foraging behavior of birds and fish. The second technique, the gray wolf optimization (GWO), is based on the hierarchical leadership and hunting mechanisms observed in gray wolves. Lastly, the firefly algorithm (FA) takes cues from the luminous flashes and movement patterns of fireflies. It incorporates mechanisms used for attracting mates and hunting. Initially, the bioinspired methods are used to perform a global search, traversing the entire operating space of the characteristic curves. After completing the search iterations, the P&O method with a small perturbation step is employed to refine the operating point for the hybrid approaches.

For current prediction, the value is derived from the mathematical modeling of the DC-DC boost converter. This involves considering the input voltage (V_{in}) as the PV voltage, a selected load (R) to achieve maximum power at the desired output voltage (V_o), the converter static gain (G), and its duty cycle (D). The static gain (G) can be expressed as follows:

$$G = \frac{V_o}{V_{in}} = \frac{1}{1-D} \tag{1}$$

Equations (2) and (3) represent the current flowing through the load (R) and the current passing through the inductor (L), respectively.

$$I_R = \frac{V_o}{R} \tag{2}$$

$$I_L = \frac{I_D}{1-D} \tag{3}$$

Where (I_D) is the current in the converter diode, which in average terms is the same as (I_R). Thus, isolating (I_D) in (3) and equating it to (2) yields (4).

$$I_L = \frac{V_o}{R(1-D)} \tag{4}$$

In the method, a voltage sensor is used to measure (V_{in}). Thus, from (1), it is possible to isolate (V_o) and replace it in (4), deriving (5).

$$I_L = \frac{V_{in}}{R(1-D)^2} = I_{PV} \tag{5}$$

Equation (5) represents the predicted input current of the photovoltaic system, which is used for processing the MPPT algorithms. It is worth mentioning that the methodology addressed in this work requires an estimate of the load at the MPP. The current estimator operates in steady state, using only average values for prediction. As a result, the capacitor current has no impact on estimation.

A. *Particle Swarm Optimization - PSO*

The PSO method is an evolutionary algorithm applied to optimize multivariable functions with numerous local optima [12]. Its modeling is based on the foraging of a flock of birds and a school of fish. In this algorithm, a population of N particles is defined, each characterized by its position (x_i) and velocity (v_i) which are updated at each iteration. It is observed that for the first iteration, the position of each particle is randomly assigned within the search space, while its velocity is set within the interval [0, 1]. In addition, each particle has its fitness value defined by an objective function. During the search process, the position of the particles is influenced by the best position found individually by the particle (p_{best}) and by the best position of the entire population (g_{best}). In this sense, the position (x_i) of the particles is adjusted according to (6).

$$x_i(k+1) = x_i(k) + v_i(k+1) \tag{6}$$

With the speed (v_i) calculated by (7).

$$v_i(k+1) = \omega v_i(k) + c_1 r_1 \left(p_{best,i} - x_i(k)\right) + c_2 r_2 \cdot \left(g_{best} - x_i(k)\right) \quad (7)$$

Where (ω) is the inertia weight; (r_1) and (r_2) are random variables between [0, 1]; (c_1) and (c_2) are acceleration coefficients that measure the importance of p_{best} and g_{best} values. To exemplify, when $c_1 = c_2$, both values are equally considered to define the particles velocity. Furthermore, (k) is the number of iterations. The search process ends when the iteration limit value is reached, or when some convergence criterion is reached.

Figure 3 illustrates the flowchart of the PSO method. The process begins by defining the population size and the maximum number of iterations. Each particle is then randomly positioned within the range [0, Voc], where Voc represents the open-circuit voltage of the array. Next, the fitness value of each particle is calculated using the extracted power as the objective function, as shown in (8).

$$f(x_i) = P_i^k = V_i^k \cdot I_i^k \quad (8)$$

Where (V) and (I) are the voltage and current of the photovoltaic array of particle (i) in iteration (k). The power of the current iteration $\left(P_i^k\right)$ is compared with the power obtained in the previous iteration $\left(P_i^{k-1}\right)$. If $\left(P_i^k\right)$ is greater, it is set as $\left(P_{best,i}\right)$. After evaluating all particles, (g_{best}) is defined as the position of the particle that achieved the highest power. These constraints are used for the particle update process according to (6) and (7).

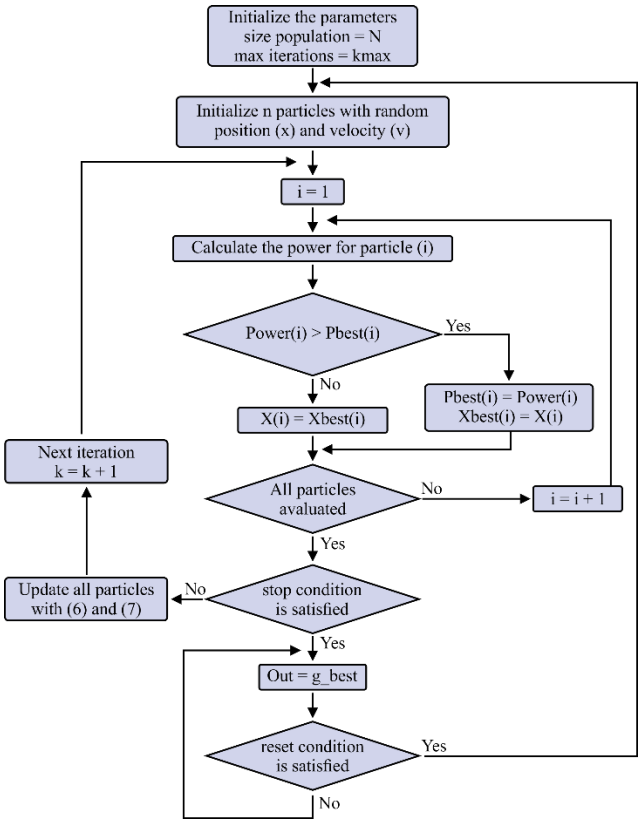

FIGURE 3. PSO based MPPT Flowchart.

The stopping condition is met when the algorithm reaches the iteration limit or if the particle speed falls below a specified threshold. Furthermore, the reset condition identifies changes in irradiance and temperature values, which affect the MPP; Thus, (9) determines whether the algorithm should be restarted [13].

$$\frac{P_{gbest} - P_{last}}{P_{last}} > \Delta P\ (\%) \quad (9)$$

Where (ΔP) is the power variation limit chosen by the designer, (P_{gbest}) is the power at the best point found by the swarm and (P_{last}) is the power recorded in each iteration after convergence.

B. *Firefly Algorithm - FA*

The FA method, proposed by Yang in 2009 [14], is based on the light emission mechanism that fireflies use to attract prey, mates, and signal danger. The emitted light is directly related to the physical characteristics of each firefly, meaning that each individual has a different intensity. Consequently, brighter fireflies have an advantage over those with lower luminosity. Thus the algorithm is based on the principle that light decreases as the distance from the light source increases [15]. The flashing light of fireflies is modeled to correspond with an objective function, enabling the solution of optimization problems, similar to the PSO method. In this context, the formulation of the algorithm is based on three key assumptions:

1) All fireflies are unisex, so a firefly will be attracted to the brightest one until it is compared to all fireflies;
2) Attractiveness is proportionally related to relative brightness, both being inversely proportional to frequency ranges;
3) The brightness of each firefly is determined by the objective function $f(x_i)$.

In the mathematical formulation, attractiveness is related to both the brightness of the fireflies and their distance. Specifically, as the distance increases, the brightness decreases, resulting in weaker attraction. This relationship is represented by (10).

$$\beta = \beta_0 e^{-\gamma r_{ij}^2} \quad (10)$$

Where (β_0) is the initial attractiveness, usually set to 1, (r_{ij}) is the Cartesian distance between two fireflies, calculated by (11) and (γ) is the absorption coefficient that controls the rate at which brightness intensity decreases.

$$r_{ij} = \left\|x_i - x_j\right\| = \sqrt{\sum_{k=1}^{d}\left(x_{i,k} - x_{j,k}\right)^2} \quad (11)$$

$$x_i^{k+1} = x_i^k + \beta \cdot \left(x_j^k - x_i^k\right) + \alpha \cdot \left(rand - \frac{1}{2}\right) \quad (12)$$

Equation (12) calculates the movement of one firefly toward another, with the attraction between firefly (i) and firefly (j) represented by the second term of (12). A random number between 0 and 1, $(rand)$, is used to assist the algorithm in traversing the entire search space, as can be seen in the third term [14].

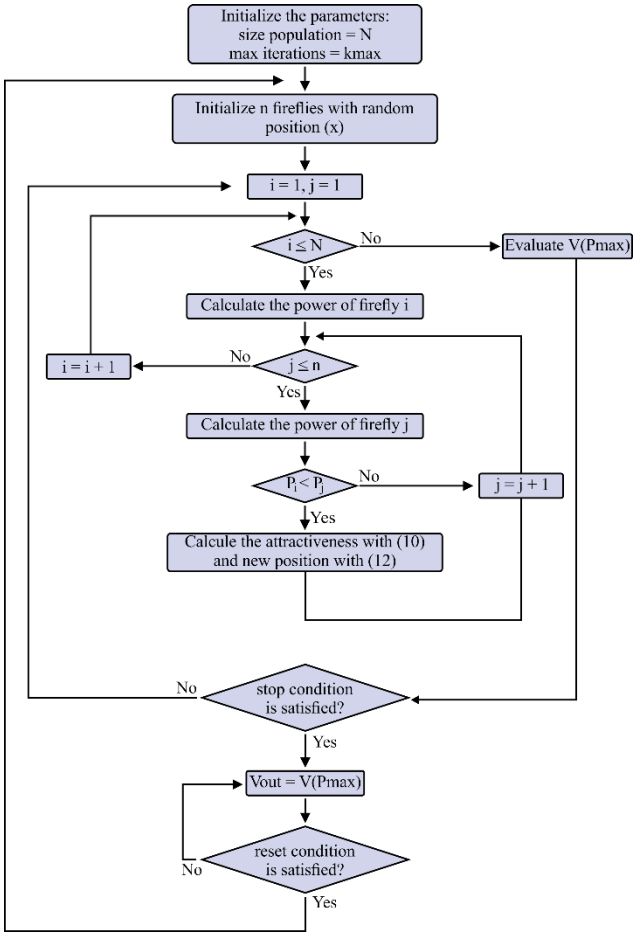

FIGURE 4. FA based MPPT Flowchart

The FA-based MPPT technique is illustrated in the flowchart shown in Figure 4. Similar to the PSO method, initially a population of N individuals is generated, all with their brightness evaluated from (8); later, each firefly is compared with the others and moves towards the brightest. To exemplify, suppose fireflies (i) and (j), respectively positioned in (x_i) and (x_j). If the brightness of firefly (j) is greater than the brightness of (i), (x_i) is updated towards (x_j), and a new fitness value is calculated; otherwise, the position of the firefly (i) remains unchanged. The comparison process ends after all fireflies have been compared to each other, and a new iteration begins. The algorithm concludes after completing the specified number of iterations and is restarted when the condition in (9) is met.

C. *Grey Wolf Optimization - GWO*

Inspired by the hunting behavior of gray wolves, Mirjalili proposed the GWO algorithm in 2014 [16]. The algorithm models the hierarchical organization of the pack during the hunt. Within the leadership hierarchy, four types of wolves are considered: Alpha, Beta, Delta, and Omegas. Alpha (α) is the wolf best located in the hunting search space, responsible for making decisions and leading the pack. Beta (β) and Delta (δ) are the second and third in command, respectively. They must submit to (α) and help in decision-making, while the Omegas (ω) are the other members of the pack. Having no decision-making power to move the pack, they perform various tasks, such as caring for sick and injured wolves and signaling dangerous situations to the pack. Equations (13) and (14) mathematically model the behavior of surrounding prey during hunting.

$$\vec{D} = \left|\vec{C} \cdot \vec{X}_p - \vec{X}(k)\right| \tag{13}$$

$$\vec{X}(k+1) = \vec{X}_p(k) - \vec{A} \cdot \vec{D} \tag{14}$$

Where $(\vec{X}_p)$ indicates the prey position vector, $(\vec{X})$ the gray wolf position vector. $(\vec{A})$ and $(\vec{C})$ represent the coefficient vectors, calculated as follows:

$$A = 2a \cdot r_1 - a \tag{15}$$

$$C = 2 \cdot r_2 \tag{16}$$

Here (r_1) and (r_2) are randomness vectors defined within the interval [0,1]. (a) is used as a convergence factor which decreases from 2 to 0, depending on the relationship between the current iteration (k) and the maximum number of iterations (k_{max}), as described by (17).

$$a = 2 \cdot \left(1 - \frac{k}{k_{max}}\right) \tag{17}$$

To update the wolves' positions, it is necessary to perform (18) to (24), as follows:

$$D_\alpha = \left|C_1 \cdot X_\alpha - X_{wolf}(k)\right| \tag{18}$$

$$D_\beta = \left|C_2 \cdot X_\beta - X_{wolf}(k)\right| \tag{19}$$

$$D_\delta = \left|C_3 \cdot X_\delta - X_{wolf}(k)\right| \tag{20}$$

$$X_{wolf,\alpha} = X_\alpha - A_1 \cdot D_\alpha \tag{21}$$

$$X_{wolf,\beta} = X_\beta - A_2 \cdot D_\beta \tag{22}$$

$$X_{wolf,\delta} = X_\delta - A_3 \cdot D_\delta \tag{23}$$

$$X_{wolf}^{k+1} = \frac{X_{wolf,\alpha} + X_{wolf,\beta} + X_{wolf,\delta}}{3} \tag{24}$$

Where $(D_\alpha), (D_\beta), (D_\delta)$ are the distances between the positions of the wolves that dictate the movement of the pack (X_α), (X_β) and (X_δ) in relation to the position of the wolf $X_{wolf}(k)$. The position of each wolf in the following iteration, $X_{wolf}(k+1)$ is given by the average of the positions evaluated by the wolves in the command, respectively expressed by $(X_{wolf,\alpha}), (X_{wolf,\beta})$ and $(X_{wolf,\delta})$ [17, 18].

The flowchart of the GWO method is shown in Figure 5. The pack is initiated by defining N individuals and a maximum number of iterations. Each wolf randomly receives a position within the search space [0, Voc] and the power is calculated by (8). Then, a descending order is established, where the first three wolves are defined by $(\alpha), (\beta)$, and (δ), respectively. Then, the position of each wolf is updated through (24) until the stopping criterion is reached, which is typically defined by the maximum number of iterations. Furthermore, reinitialization occurs when (9) is satisfied.

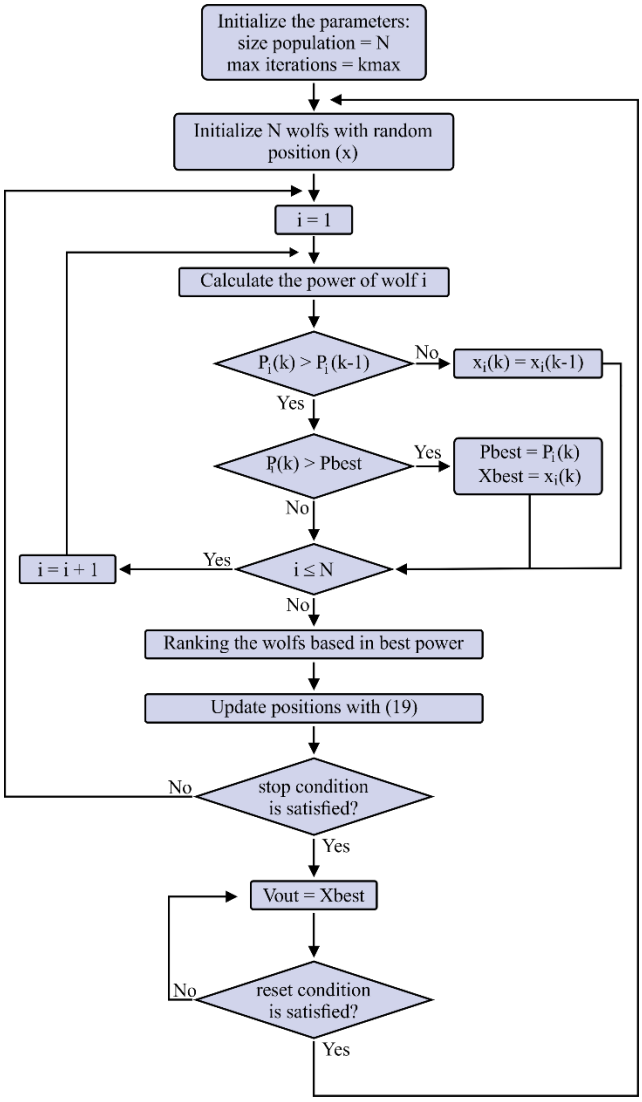

FIGURE 5. GWO based MPPT Flowchart.

D. *Perturb and Observe – P&O*

The flowchart of the P&O algorithm is presented in Figure 6. The method begins its operation by evaluating the power generated by the photovoltaic array. Next, the array voltage is adjusted, either increased or decreased. After this adjustment, a new evaluation is performed, and the resulting power is compared with the value obtained in the previous iteration. If the power in the current iteration, denoted as $P(k)$, is greater than the power in the previous iteration, $P(k-1)$, this indicates that the perturbation was effective. Consequently, the same perturbation direction is maintained to continue the search for the MPP. Conversely, if the power in the current iteration is less than the power in the previous iteration, then the perturbation direction should be changed to the opposite direction [19].

Finally, hybrid techniques can combine the P&O method with each of the metaheuristics described so far, resulting in PSO-P&O, FA-P&O and GWO-P&O. The methodology adopted to search for the MPP will begin with the intelligent algorithm, performing a broad sweep of the search space, then the P&O algorithm will be used to refine the point found resulting in an operation with small variations around the MPP. The objective is to reduce the number of iterations required by each intelligent technique and, consequently, decrease the convergence time.

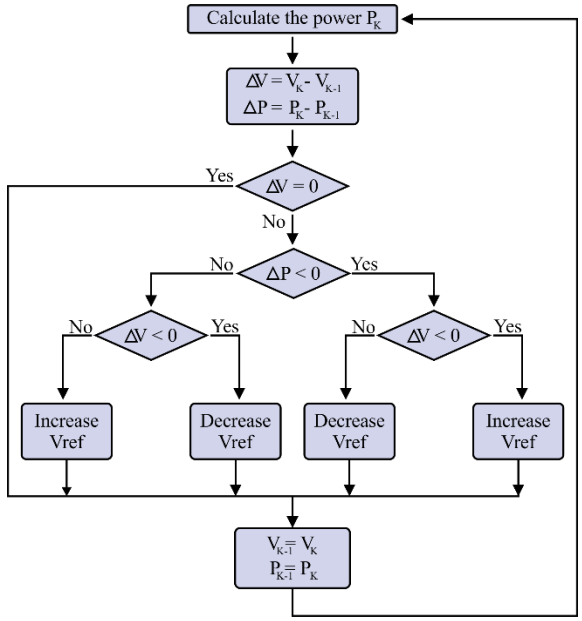

FIGURE 6. P&O based MPPT Flowchart.

As pointed out before, traditional methodologies rely on both current and voltage sensors to accurately calculate power extraction. In our proposal, however, precise current values are not necessary. Instead, the focus is on verifying power changes using the objective functions of metaheuristic algorithms. In that sense, a steady state current estimator is sufficient to satisfactory results.

Alternatively, a dynamic current estimator could be used [20, 21]. However, an additional voltage sensor and its circuitry must be added to the system. Furthermore, specific data, such as the equivalent series resistance of the inductor and/or parasitic components losses must be included in the control system, which may vary in practice due to heating.

III. SIMULATION RESULTS

Figure 7 illustrates the simulation model developed in the MATLAB/Simulink® environment to implement the proposed algorithms. The solar cell model used is described by [22], and each MPPT technique, implemented as an m-function, is employed to control the duty cycle of the DC-DC boost converter.

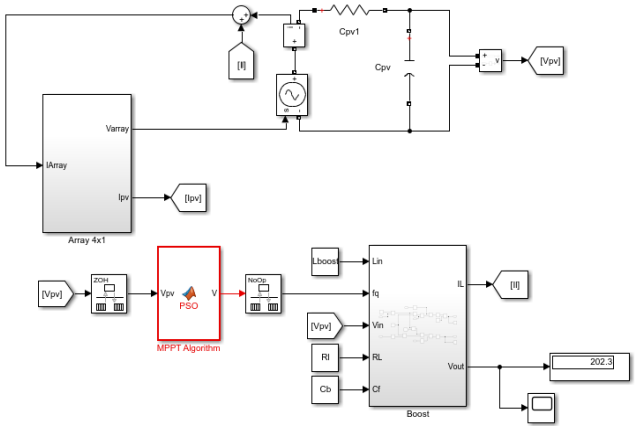

FIGURA 7. MATLAB/Simulink® Simulation Model.

The boost converter is modeled using its average model [2], with the following specifications: inductance L_b = 3.3

mH, output capacitance C_b = 27 µF, load resistance R_L = 50 Ω, and a switching frequency of f_s = 20 kHz. The PI controller was tuned according to [23] resulting in k_p = 0.001 and ki = 3.48.

Table 1 presents the parameters of each irradiation and temperature step used in the simulation of the evaluated methods, along with the maximum theoretical power. The photovoltaic array consists of 4 series-connected KC200GT modules.

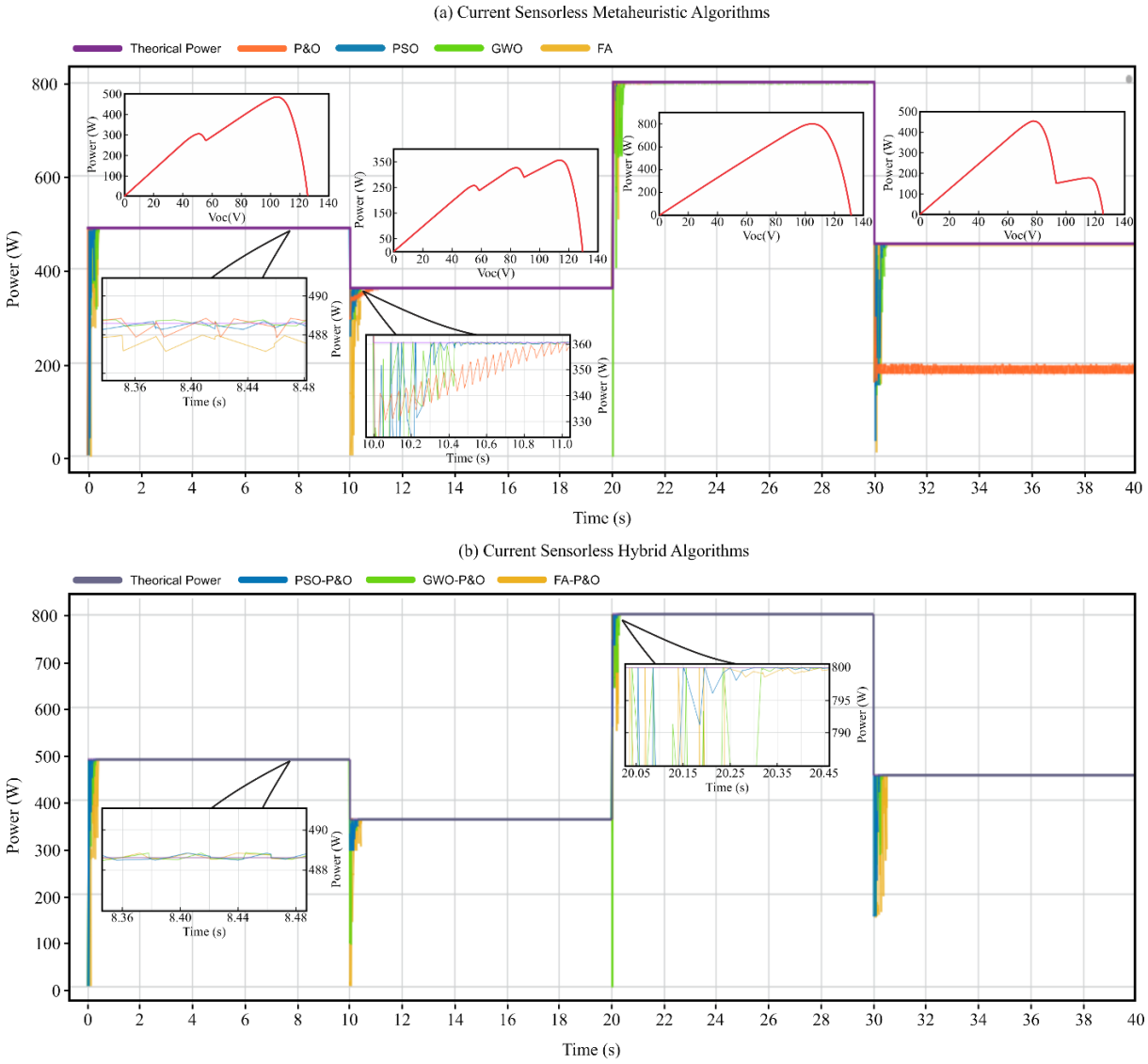

FIGURE 8. Power Extracted using the Current Sensorless Algorithms.

TABLE 1. Varying power profiles simulation.

Irradiance (W/m²) M1; M2; M3; M4	Temperature (°C)	Theorical Power (W)
600; 600; 800; 800	35	488.60
400; 500; 600; 700	20	360.56
1000; 1000; 1000; 1000	25	800.04
200; 750; 750; 900	30	454.53

To simulate the PSO algorithm, varying coefficients were used. As proposed in [24], equations (25), (26), and (27) are applied to adjust the learning coefficients and inertia weight according to the number of iterations.

$$c_1 = c_{1,max} - (c_{1,max} - c_{1,min}) * \left(\frac{k}{k_{max}}\right) \quad (25)$$

$$c_2 = c_{2,min} + (c_{2,max} - c_{2,min}) * \left(\frac{k}{k_{max}}\right) \quad (26)$$

$$\omega = \omega_{max} - (\omega_{max} - \omega_{min}) * \left(\frac{k}{k_{max}}\right) \quad (27)$$

It is observed that the parameters (c_1) and (ω) are initially set to the maximum value to assist in a broad search, refining the particle movement as the number of iterations increases; while (c_2) is used to reduce oscillations close to the MPP. Table 2 presents the adopted parameters.

TABLE 2. PSO parameters.

$c_{1,max}$	2.00	$c_{1,min}$	0.6
$c_{2,max}$	2.20	$c_{2,min}$	0.4
ω_{max}	0.60	ω_{min}	0.2
k_{max}	25	N	5

In [25], a modified FA method is proposed, which evaluates solutions similarly to those used for the PSO algorithm, applying equations (28) and (29) to express the values of (β_0) and (α) as a function of the number of algorithm iterations.

$$\alpha = \alpha_{max} + (\alpha_{min} - \alpha_{max}) * \left(\frac{k}{k_{max}}\right) \quad (28)$$

$$\beta_0 = \beta_{0max} + \left(\beta_{0min} - \beta_{0max}\right) * \left(\frac{k}{k_{max}}\right) \quad (29)$$

The parameter (α) assists in the randomization of the search space in a directly proportional manner. Specifically, the higher the value of (α), the greater the exploration carried out by the fireflies, consequently the lower the convergence speed. Thus, small values of (α) result in a more refined search, which increases the risk of convergence to local maxima. The parameter (β_0) is also related to the convergence time, exhibiting an inversely proportional relationship [25]. The coefficients used to simulate the FA method are shown in Table 3.

TABLE 3. FA parameters.

α_{max}	0.65	α_{min}	0.17
β_{max}	2.60	β_{min}	1.15
k_{max}	15	N	3

For the GWO method, the modification proposed in [18] was used, which assigns different weights to the wolves $(\alpha), (\beta)$ and (δ), as shown in (30). Unlike equation (24), which applies equal weights to wolves with decision-making influence, which ends up ignoring the difference that exists between them. The simulation of the GWO method is defined with $N = 3$ and $k_{max} = 15$.

$$X_{wolf}^{(k+1)} = \frac{X_{wolf,\alpha}}{2} + \frac{X_{wolf,\beta}}{3} + \frac{X_{wolf,\delta}}{6} \quad (30)$$

Figure 8(a) illustrates the power extracted from the array using the Current Sensorless P&O [10], Current Sensorless PSO, Current Sensorless GWO, and Current Sensorless FA algorithms, all of which include current prediction. The Tracking Factors (TFs) for the algorithms are 87.08%, 99.59%, 99.30%, and 99.11%, respectively. It is worth mentioning that the Current Sensorless P&O algorithm, which lacks a global maximum search feature does not accurately track the ideal MPP, as can be seen in the last profile where the method converges to a local maximum.

Furthermore, each method was combined with the P&O algorithm to create three other hybrid algorithms. To minimize oscillations around the MPP, the P&O perturbation was set to 0.1 V. Thus, in Figure 8(b) the power extracted is evaluated with the hybrid methods Current Sensorless PSO-P&O, Current Sensorless FA-P&O and Current Sensorless GWO-P&O. The TFs for the algorithms are 99.75%, 99.53%, and 99.22%, respectively. The hybrid methods have a reduction of 5 iterations, except for the FA method, which maintained the same number of iterations. All methods achieved superior efficiency compared to those that are not combined with the P&O algorithm, both by reducing the number of iterations and by refining the operation around the MPP, which can be observed by evaluating the details in Figures 8(a) and 8(b). It is worth mentioning that all algorithms work with an acquisition frequency of 1 kHz and a crossover frequency of 100 Hz. The PI controller tuning followed the strategy outlined in [26].

Figures 9, 10, and 11 show the comparison between the sensorless hybrid algorithms and the algorithms using both current and voltage sensors. For this, the same coefficients were applied as in the first simulation profile of Table 1.

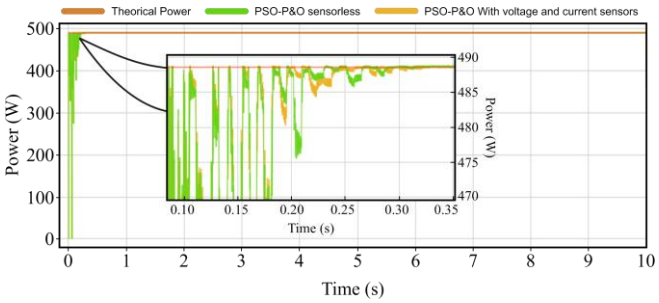

FIGURE 9. Comparison of Power Extracted for PSO-P&O Current Sensorless and PSO-P&O With voltage and current sensors.

The TFs for the PSO-P&O Current Sensorless and PSO-P&O algorithms with both sensors are, respectively, 99.77% and 99.78%, with a convergence time of around 0.33s.

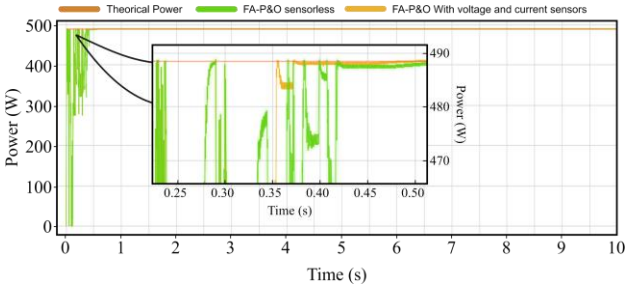

FIGURE 10. Comparison of Power Extracted for FA-P&O Current Sensorless and FA-P&O With voltage and current sensors.

The TFs for the FA-P&O Current Sensorless and FA-P&O algorithms with both sensors are, respectively, 99.06% and 99.10%, with a convergence time of around 0.50s.

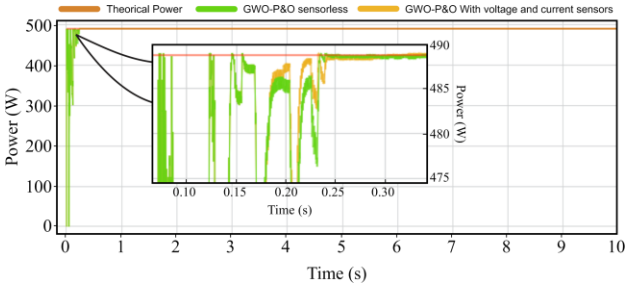

FIGURA 11. Comparison of Power Extracted using GWO-P&O Current Sensorless and GWO-P&O With voltage and current sensors.

The TFs for the GWO-P&O Current Sensorless and GWO-P&O algorithms with both sensors are, respectively, 99.69% and 99.70%, with a convergence time of around 0.30s.

To simplify the comparison between the MPPT algorithms, Table 4 provides a concise analysis, offering an

overview of their main characteristics and performance according to the applied irradiance and temperature profiles.

Additionally, to evaluate the performance of the algorithms under conditions of inaccurate current estimation, the PSO sensorless algorithm was tested with measurement errors of 5% and 10% in the current. For this, the load value was changed in the software to a range of -10% and + 10%. The tested power profile remains the same as shown in Table 1. The tracking factors achieved were 99.56%, 99.59%, 99.57, and 99.60, for -5%, -10%, +5%, and +10% errors, respectively. Therefore, the algorithms are not directly influenced by current estimation errors as the main purpose of their cost functions is to verify the increase in power extraction rather than the exact power measurement.

TABLE 4. Comparison of the MPPT techniques considering the four applied power profiles.

	Search Time for the GMPP (s)				Steady-State Power Oscillation (%)				Tracking Efficiency (%)				TF (%)
Case	1	2	3	4	1	2	3	4	1	2	3	4	Global
P&O Sensorless	0.05	1.40	0.20	-	0.13	0.43	0.22	2.20	100	100	100	40.70	87.07
PSO Sensorless	0.35	0.40	0.21	0.45	0.10	0.16	0,03	0,06	100	100	100	100	99.59
GWO Sensorless	0.50	0.46	0.47	0.52	0.05	0.14	0.14	0.15	100	100	100	100	99.30
FA Sensorless	0.51	0.40	0.28	0.32	0.06	0.14	0.04	0,13	99.77	100	100	99.48	99.11
P&O+PSO Sensorless	0.30	0.28	0.28	0.24	0.04	0.05	0.01	0.04	100	100	100	100	99.75
P&O+GWO Sensorless	0.34	0.32	0.34	0.35	0.08	0.13	0.02	0.04	100	100	100	100	99.53
P&O+FA Sensorless	0.51	0.48	0.25	0.52	0.04	0.05	0.01	0,02	100	100	100	100	99.22

(-) GMPP not found.

Thus, for the construction of Table 4, criteria such as GMPP search time, steady-state power oscillation, tracking efficiency, and TF were considered. Each metric is detailed below [27,28]:

1) **GMPP search time:** This refers to the time it takes for the algorithm to locate the GMPP. This criterion is crucial, as a longer search time implies lower energy yield;
2) **Steady-state power oscillation:** Calculated from the amplitude of the oscillations that occur after the system finds the GMPP;
3) **Tracking efficiency:** Measured by the proportion of energy obtained relative to the available energy in steady-state conditions, indicating the method's accuracy;
4) **TF (Tracking Factor):** The ratio between the useful energy extracted and the available energy over a given period, representing the overall efficiency of the system.

It is observed that the longer an irradiance and temperature profile is applied, the less influence the search time has on the calculation of the TF. Thus, in steady-state conditions, this coefficient tends to reflect the tracking efficiency, which is related to how closely the system operates at the GMPP. As a highlight of the simulation results, the P&O+PSO sensorless and P&O+GWO sensorless algorithms achieved the highest TFs, with 99.75% and 99.53%, respectively. Both algorithms successfully tracked the GMPP in all applied profiles, with a search time of less than 0.30 s for the P&O+PSO sensorless and less than 0.35 s for the P&O+GWO sensorless.

IV. EXPERIMENTAL RESULTS

Figure 12 presents the experimental model developed. A programmable power source, the TerraSAS ETS 600/17 model by Elgar, is used to simulate the electrical behavior of photovoltaic modules. The software for this source allows for the configuration of photovoltaic arrays and enables the insertion of parameters for systems with partial shading. The TerraSAS is configured to match the photovoltaic array used during the simulation and is then connected to the DC-DC boost converter. Additionally, the TMS320F28379D DSP by Texas Instruments is used to control the converter by processing signals obtained from the current and voltage sensors through signal conditioning circuitry. The boost switch is G4PH50UD, the boost diode is RHRP860, the inductor core is an NEE 65/33/39. The voltage sensor is LV 25-P LEM.

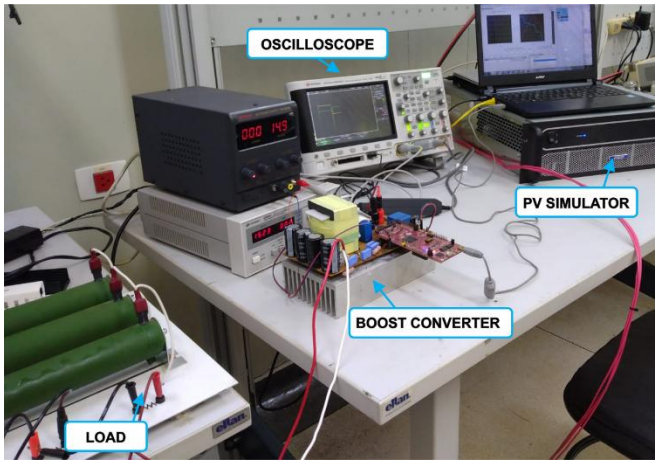

FIGURE 12. Experimental setup implementation.

Neglecting the usage of a hall effect sensor and its conditioning circuitry, we may reduce the prototype cost by approximately US$ 37.16.

For the experiment, four new power profiles were applied, as shown in Table 5.

TABLE 5. Experimental varying power profiles.

Irradiance (W/m²) M1; M2; M3; M4	Temperature (°C)	Theorical Power (W)
750; 650; 580; 360	10	394.50
900; 800; 900; 800	25	665.20
200; 750; 750; 900	30	454.65
1000; 600; 1000; 600	35	499.20

Each profile is applied for 40 seconds, during which the oscilloscope is used to monitor the waveforms of power, current, and voltage from the photovoltaic array. The experimental results for the PSO algorithm are then shown in Figures 13 and 14 for both sensor and sensorless methods, respectively.

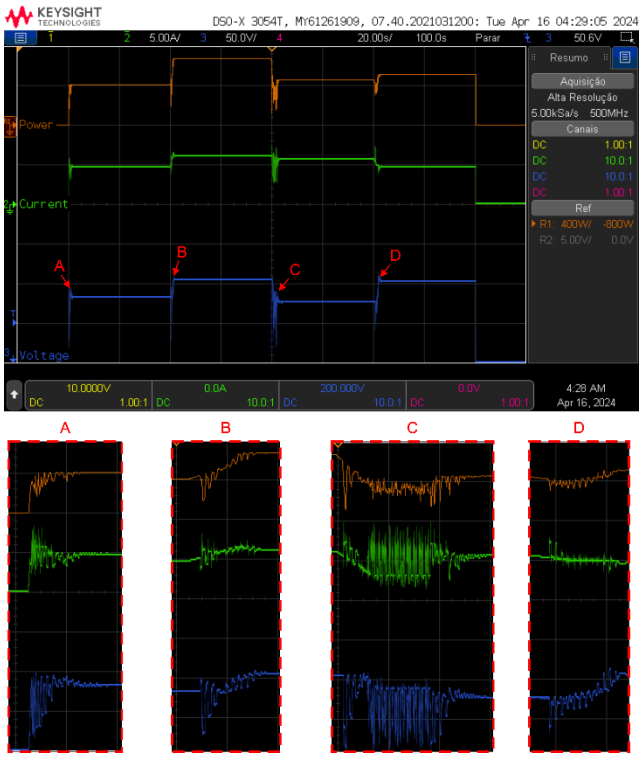

FIGURE 13. Power Extracted for experimental PSO with voltage and current sensors.

In Figures 13 and 14, the power of the photovoltaic array is shown in orange (400W/div); the current in green (5A/div), and the voltage in blue (50V/div). The detailed views, with time scale of 1s/div, reveal the behavior of the system during transitions between power profiles. It is noted that both methods found the GMPP in all evaluated profiles. The TFs for the algorithm with both sensors are 99.03% and 99.08% for the sensorless algorithm. Furthermore, a search time between 1.35 and 2.50 seconds is observed, considering all the applied steps. The parameters of the PSO algorithm used in the experiments are listed in Table 6.

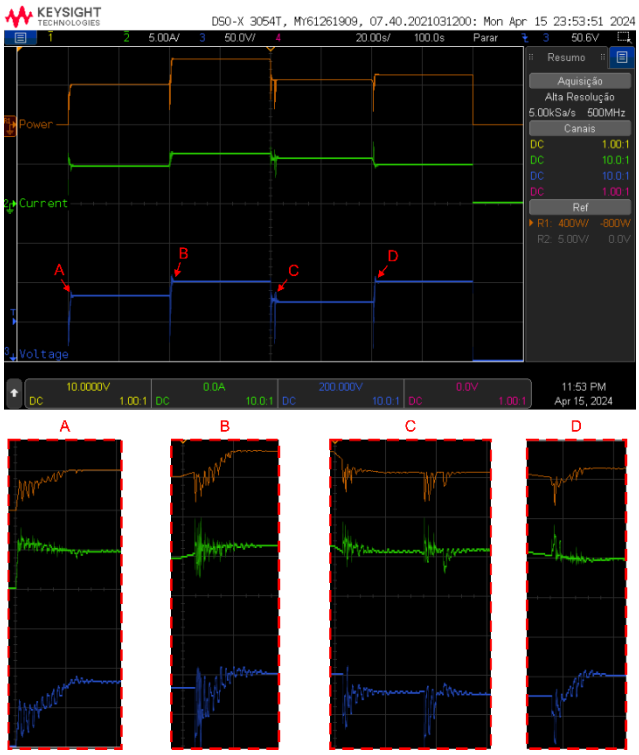

FIGURE 14. Power Extracted for experimental Current Sensorless PSO.

TABLE 6. PSO experimental parameters.

$c_{1,max}$	2.20	$c_{1,min}$	0.15
$c_{2,max}$	2.20	$c_{2,min}$	0.57
ω_{max}	0.60	ω_{min}	0.20
k_{max}	20	N	4

V. CONCLUSIONS

This work presented three Current Sensorless Global maximum power point tracking algorithms that do not require current sensors. They are Current Sensorless PSO, Current Sensorless FA, and Current Sensorless GWO. Instead, these algorithms rely solely on a single voltage sensor at the input and incorporate duty cycle feedback to estimate current, along with compensators for optimization purposes. Additionally, each of the three methods was combined with the P&O algorithm, resulting in three hybrid algorithms: Current Sensorless PSO-P&O, Current Sensorless FA-P&O, and Current Sensorless GWO-P&O. Simulation and experimental results demonstrated that the algorithms achieved excellent performance in terms of tracking maximum power with high convergence speed, maintaining the same level of quality as algorithms that use both sensors. Among the algorithms, Current Sensorless PSO+P&O stood out with the highest TF for the scenarios tested during the simulations. Furthermore, the experimental results also demonstrate that the applied sensorless methodology is capable of tracking the GMPP and achieving a higher TF compared to the conventional methodology that uses both sensors.

ACKNOWLEDGMENT

The authors would like to thanks CAPES (Finance Code 001) and CNPq (process 306749/2022-0).

AUTHOR'S CONTRIBUTIONS

MARTINES, G. M. S.: Data Curation, Formal Analysis, Investigation, Methodology, Software, Validation, Visualization, Writing – Original Draft, Writing – Review & Editing. **DE BRITO, M. A. G.**: Conceptualization, Data Curation, Formal Analysis, Funding Acquisition, Investigation, Methodology, Project Administration, Resources, Supervision, Validation, Visualization, Writing – Original Draft, Writing – Review & Editing. **BATISTA, E. A.**: Investigation, Methodology, Software, Validation. **GODOY, R. B.**: Formal Analysis, Investigation, Methodology, Resources, Validation, Writing – Original Draft. **MATEUS, T. H. A.**: Investigation, Methodology, Software, Validation.

PLAGIARISM POLICY

This article was submitted to the similarity system provided by Crossref and powered by iThenticate – Similarity Check.

REFERENCES

[1] Teo, J. C. et al. Impact of partial shading on the PV characteristics and the maximum power of a photovoltaic string. Energies, v. 11, n. 7, p. 1860, 2018, doi: 10.3390/en11071860.

[2] Esram, T,; Chapman, P. L. Comparison of photovoltaic array maximum power point tracking techniques. IEEE Transactions on Energy Conversion, New York, v.24, n.2, p. 439-449, 2007, doi: 10.1109/TEC.2006.874230.

[3] Faranda, R.; Leva, S.; Maugeri, V. MPPT techniques for PV systems: Energetic and cost comparison. In: POWER AND ENERGY SOCIETY GENERAL MEETING - PESGM, 9., 2008, Pittsburgh. Proceedings… Pittsburgh: IEEE, 2008. p. 1-6. doi: 10.1109/PES.2008.4596156

[4] Jain, S.; Agarwal, V. Comparison of the performance of maximum power point tracking schemes applied to single-stage grid-connected photovoltaic systems. IET Electric Power Applications, United Kingdom, v. 3, n. 3, p. 753-762, 2007. doi: 10.1049/iet-epa:20060475

[5] Tepe, Izviye Fatimanur; Irmak, Erdal. Review and comparative analysis of metaheuristic MPPT algorithms in PV systems under partial shading conditions. In: 2022 11th International Conference on Renewable Energy Research and Application (ICRERA). IEEE, 2022. p. 471-479. doi: 10.1109/ICRERA55966.2022.9922868.

[6] Dziri, Samia et al. Improved Particle Swarm Optimizer-Based MPPT Control of PV Systems Under Dynamic Partial Shading. In: 2022 19th International Multi-Conference on Systems, Signals & Devices (SSD). IEEE, 2022. p. 1603-1608. 10.1109/SSD54932.2022.9955506.

[7] Elobaid, Lina M.; ABDELSALAM, Ahmed K.; ZAKZOUK, Ezeldin E. Artificial neural network-based photovoltaic maximum power point tracking techniques: a survey. IET Renewable Power Generation, v. 9, n. 8, p. 1043-1063, 2015. doi: 10.1049/iet-rpg.2014.0359.

[8] Karatepe, E. et al. Artificial neural network-polar coordinated fuzzy controller based maximum power point tracking control under partially shaded conditions. IET Renewable Power Generation, v. 3, n. 2, p. 239-253, 2009. doi: 10.1049%2Fiet-rpg%3A20080065.

[9] A. Mani, S. K and S. Maiti, "A Novel Hybrid Global MPPT Technique for Grid connected PV Systems," 2021 National Power Electronics Conference (NPEC), Bhubaneswar, India, 2021, pp. 1-6, doi: 10.1109/NPEC52100.2021.9672489.

[10] De Brito, M. A. G.; Martines, G. M. S.; Volpato, A. S.; Godoy, R. B.; Batista, E. A. Current Sensorless Based on PI MPPT Algorithms. Sensors 2023, 23, 4587. https://doi.org/10.3390/s23104587.

[11] De Brito, Moacyr A. G. et al. Current Sensorless MPPT Algorithms for PV Systems with Partial Shading. In: 2023 IEEE 8th Southern Power Electronics Conference (SPEC). IEEE, 2023. p. 1-8. doi: 10.1109/SPEC56436.2023.10408140.

[12] Kennedy, James; Eberhart, Russell. Particle swarm optimization. In: Proceedings of ICNN'95-international conference on neural networks. IEEE, 1995. p. 1942-1948. doi: 10.1109/ICNN.1995.488968.

[13] Alshareef, Muhannad et al. Accelerated particle swarm optimization for photovoltaic maximum power point tracking under partial shading conditions. Energies, v. 12, n. 4, p. 623, 2019. doi: 10.3390/en12040623.

[14] Yang, Xin-She. Firefly algorithms for multimodal optimization. In: International symposium on stochastic algorithms. Berlin, Heidelberg: Springer Berlin Heidelberg, 2009. p. 169-178. doi: 10.1007/978-3-642-04944-6_14.

[15] Watanabe, Rodrigo Bairros et al. Implementation of the Bio-Inspired Metaheuristic Firefly Algorithm (FA) Applied to Maximum Power Point Tracking of Photovoltaic Systems. Energies, v. 15, n. 15, p. 5338, 2022. doi: 10.3390/en15155338.

[16] Mirjalili, Seyedali; Mirjalili, Seyed Mohammad; Lewis, Andrew. Grey wolf optimizer. Advances in engineering software, v. 69, p. 46-61, 2014. doi: 10.1016/j.advengsoft.2013.12.007.

[17] Mohanty, Satyajit; Subudhi, Bidyadhar; Ray, Pravat Kumar. A new MPPT design using grey wolf optimization technique for photovoltaic system under partial shading conditions. IEEE Transactions on Sustainable Energy, v. 7, n. 1, p. 181-188, 2015. doi: 10.1109/TSTE.2015.2482120.

[18] Millah, Ibrahim Saiful et al. An enhanced grey wolf optimization algorithm for photovoltaic maximum power point tracking control under partial shading conditions. IEEE Open Journal of the Industrial Electronics Society, v. 3, p. 392-408, 2022. doi: 10.1109/OJIES.2022.3179284.

[19] Brito, M. A. G.; Sampaio, L. P.; Galotto Junior, L.; Canesin, Carlos Alberto. Evaluation of the Main MPPT Techniques for Photovoltaic Applications. IEEE Transactions on Industrial Electronics (1982. Print), v. 60, p. 1156-1167, 2013. doi: 10.1109/TIE.2012.2198036.

[20] G. Cimini, G. Ippoliti, G. Orlando, S. Longhi and R. Miceli, "Robust current observer design for DC-DC converters," 2014 International Conference on Renewable Energy Research and Application (ICRERA), Milwaukee, WI, USA, 2014, pp. 958-963, doi: 10.1109/ICRERA.2014.7016527.

[21] K. Biswas and O. Ray, "A Nonintrusive Digital Current Sensing Method for DC–DC Converters With Wide Load Range," in IEEE Sensors Letters, vol. 7, no. 6, pp. 1-4, June 2023, Art no. 6002704, doi: 10.1109/LSENS.2023.3276777.

[22] Casaro, M. M.; Martins, D. C. Modelo de arranjo fotovoltaico destinado a análises em eletrônica de potência via simulação. Eletrônica de Potência, v. 13, n. 3, p. 141-146, 2008. doi: 10.18618/REP.2008.3.141146.

[23] Brito, Moacyr A. G. de, Victor A. Prado, Edson A. Batista, Marcos G. Alves, and Carlos A. Canesin. 2021. "Design Procedure to Convert a Maximum Power Point Tracking Algorithm into a Loop Control System" Energies 14, no. 15: 4550. https://doi.org/10.3390/en14154550

[24] Chao, Kuei-Hsiang; Lin, Yu-Sheng; Lai, Uei-Dar. Improved particle swarm optimization for maximum power point tracking in photovoltaic module arrays. Applied energy, v. 158, p. 609-618, 2015. doi: 10.1016/j.apenergy.2015.08.047.

[25] Farzaneh, Javad; Keypour, Reza; Khanesar, Mojtaba Ahmadieh. A new maximum power point tracking based on modified firefly algorithm for PV system under partial shading conditions. Technology and Economics of Smart Grids and Sustainable Energy, v. 3, p. 1-13, 2018. doi: 10.1007/s40866-018-0048-7.

[26] De Brito, Moacyr A. G.; Batista, E. A.; Prado, V. A.; Alves, M. G.; Canesin, C. A. . Design Procedure to Convert a Maximum Power Point Tracking Algorithm into a Loop Control System. Energies, v. 14, p. 4550, 2021. doi: 10.3390/en14154550.

[27] Da Rocha, Maykon Vichoski; Sampaio, Leonardo Poltronieri; Da Silva, Sérgio Augusto Oliveira. Comparative analysis of ABC,

Bat, GWO and PSO algorithms for MPPT in PV systems. In: 2019 8th international conference on renewable energy research and applications (ICRERA). IEEE, 2019. p. 347-352. doi: 10.1109/ICRERA47325.2019.8996520.

[28] Hanzaei, Saeed H.; Gorji, Saman A.; Ektesabi, Mehran. A scheme-based review of MPPT techniques with respect to input variables including solar irradiance and PV arrays' temperature. IEEE Access, v. 8, p. 182229-182239, 2020. doi:10.1109/ACCESS.2020.3028580.

BIOGRAPHIES

Moacyr A. G. de Brito was born in Andradina, Brazil, in 1982. He received the B.S., MSc. and Ph.D degrees all in electrical engineering from São Paulo State University, Ilha Solteira, Brazil, in 2005, 2008 and 2013, respectively. He received the Best Thesis award of UNESP 2013. During his carrier he received three best paper awards at the conferences PCIM 2012, COBEP 2017 and SPEC 2018. He was Adjunct-A Professor at UTFPR from 2013 to 2016, where he was coordinator of electronic engineering under-graduation. Since 2016 he is Adjunct professor at UFMS and member of electrical engineering program and also member of BATLAB Laboratory (Artificial Intelligence, Power Electronics and Digital Control). He is currently reviewer of many Transactions Journals and Projects of FAPES and FAPESP. His interests include ballasts for fluorescent lamps, dimming control, digital control, dc-to-dc converters, switching-mode power supplies, power-factor-correction techniques, DSPs and field-programmable gate arrays, and stand-alone and grid-connected inverters. He is currently a PQ-2 CNPq productivity researcher.

Guilherme M. S. Martines was born in Campo Grande, Brazil, in 1998. He received the B.S. and M.Sc. in electrical engineering from the Federal University of Mato Grosso do Sul (UFMS). His research interests include digital control, DC-to-DC converters, neural networks, DSPs, stand-alone and grid-connected inverters. Currently, he is developing projects with commercial grid-tied photovoltaic converters.

Ruben B. Godoy holds a PhD in automation by Paulista State University, Brazil (2010). He carried out post doctorate internship in Power Electronics with the École de Technologie Supérieure, Montreal (2014). Currently, he is an Associate Professor with the Federal University of Mato Grosso do Sul, Brazil, and he works in lines of research of wireless power transfer, uninterrupted power supplies, photovoltaic water pumping, active filters and modern techniques for power metering.

Edson A. Batista was born in Ilha Solteira, SP, Brazil. He received the B.S., MSc. and Ph.D all in electrical engineering from Universidade Estadual Paulista Júlio de Mesquita Filho, in 2001, 2004 and 2009, respectively. He finishes his Post-doctoral stage (2015-2016) at the Department of Nuclear Engineering, University of Tennessee (USA), working with Predictive Controller applied to Advanced Reactors, using FPGA-in-the-Loop techniques. From 2001 to 2004, he was a Research Assistant with the Princeton Plasma Physics Laboratory. From 2009 to 2013, he has been an Assistant Professor with the Mechanical Engineering Department, Texas A&M University, liquids, spectroscopic diagnostics, plasma propulsion, and innovation plasma applications. Since 2009, he is Adjunct Professor at FAENG / UFMS and Coordinator of the Embedded Systems Laboratory - LABSEM, which contains projects funded by CNPq and FUNDECT/MS. His interests involve: Smart Grid, Intelligent Instrumentation based on IEEE 1451, Real-Time Hardware-in-the-Loop Simulation and Fractional Order Derivative Applications. He is currently the coordinator of the Graduate Program in Electrical Engineering at UFMS.

Thiago H. A. Mateus holds a Ph.D. in Electrical Engineering from the University of Campinas (2020). He has been a professor at the Federal University of Mato Grosso do Sul since 2012 and is currently the coordinator of the undergraduate program in Electrical Engineering. His main areas of expertise are Power Electronics and Artificial Intelligence. In Power Electronics, he focuses on multilevel converters connected to the power grid and photovoltaic systems. In the field of AI, he works with evolutionary algorithms, fuzzy logic, and artificial neural networks. He teaches courses on Operations Research, Systems Modeling and Simulation, Power System Analysis, and Residential and Industrial Electrical Installations.